Supplementary Information for

# Ligand-induced CaMKIIα hub Trp403 flip, hub domain stacking and modulation of kinase activity

*Dilip Narayanan[a], Anne Sofie G. Larsen[a], Stine Juul Gauger[a], Ruth Adafia[b,c], Rikke Bartschick Hammershøi[a], Louise Hamborg[a], Jesper Bruus-Jensen[a], Nane Griem-Krey[a], Christine L. Gee[d,e,f,g], Bente Frølund[a], Margaret M. Stratton[b], John Kuriyan[d,e,f,g,h,i], Jette Sandholm Kastrup[a*], Annette E. Langkilde[a*], Petrine Wellendorph[a*], Sara M. Ø. Solbak[a*]*

[a]Department of Drug Design and Pharmacology, Faculty of Health and Medical Sciences, University of Copenhagen, DK-2100 Copenhagen, Denmark; [b]Department of Biochemistry and Molecular Biology, University of Massachusetts Amherst, MA 01003; [c]Chemistry-Biology Interface Training Program, University of Massachusetts, Amherst, MA 01003, USA; [d]HHMI, University of California, Berkeley, CA 94720; [e]Department of Molecular and Cell Biology, University of California, Berkeley, CA 94720; [f]California Institute for Quantitative Biosciences, University of California, Berkeley, CA 94720; [g]Department of Biochemistry, Vanderbilt University School of Medicine, Nashville, TN 37232; [h]Department of Chemistry, University of California, Berkeley, CA 94720; [i]Physical Biosciences Division, Lawrence Berkeley National Laboratory, Berkeley, CA 94720.

[*]Main corresponding author: Sara M. Ø. Solbak, email Sara.Solbak@sund.ku.dk; corresponding author on biochemistry and pharmacology: Petrine Wellendorph, email pw@sund.ku.dk; corresponding author on SAXS: Annette E. Langkilde, email annette.langkilde@sund.ku.dk; corresponding author on X-ray crystallography: Jette S. Kastrup, email jsk@sund.ku.dk.

## Table of Contents

## Extended Materials and Methods

### 1. Cell culturing and transfection of CaMKIIα in HEK293T cells.

Human embryonic kidney (HEK) 293T (#CRL-3216, ATCC) cells were cultured as previously described (Leurs et al. 2021). In brief the cells were maintained in DMEM GlutaMAX medium (#61965026, Gibco) supplemented with 10% fetal bovine serum and 1% penicillin-streptomycin (#15140122, Invitrogen), in a humidified 5% $CO_2$ atmosphere at 37°C. HEK293T cells were transfected with rat CaMKIIα WT (pCMV6-CaMKIIα-Myc-DDK, #RR201121, Origene), generated and sequence-verified by GenScript Biotech (Leiden, the Netherlands). Transfections were performed using polyethyleneimine (PEI) (Polysciences Inc., Warrington, PA, USA). The day before transfection, cells were seeded in 10 cm culture dishes at a density of 2.0 x $10^6$. For transfection, 8 µg plasmid DNA was diluted in 970 µL serum-free medium and 24 µL 1 mg/mL PEI added. After 15 min of incubation at room temperature, the DNA/PEI mixture was added to the cells. Transfected cells were used for generating lysates for whole-cell homogenate binding, as described below. Absence of binding to cells not transfected with CaMKIIα has been reported previously (Leurs et al. 2021).

### 2. [3H]HOCPCA binding assay to whole cell homogenates.

This assay was performed as previously described (Leurs et al. 2021). The binding experiments were performed in 48-well format using glass tubes (#10682424, Corning™) with 40 nM [$^3$H]HOCPCA, 100 µg HEK293T whole cell homogenate and test compound in a total volume of 400 µL binding buffer (50 mM $KH_2PO_4$, pH 6.0). GHB (3 mM) was used for determining non-specific binding. Binding equilibrium was achieved by 1 hour incubation at 0-4 °C, followed by protein precipitation with addition of 1.6 mL acetone for 1 hour at -20 °C. Protein was collected on GF/C unifilters by rapid filtration with ice cold binding buffer using a Brandel M48-T cell harvester (Alpha Biotech). Finally, filters were submerged in 3 mL OptiFluor scintillation liquid (Perkin Elmer) to allow measurement of radioactivity (DPM) for 3 min per sample. Experiments were performed in technical triplicates and curves generated from pooled data from four individual experiments. $K_i$ values were calculated from $IC_{50}$ values using the Cheng-Prusoff equation and previously determined $K_D$ value (Leurs et al. 2021). Mean p$K_i$ values are reported as mean ± SEM.

### 3. Expression and purification of CaMKIIα hub domains.

The human CaMKIIα WT hub (UniprotKB Q9UQM7, residues 345-475), CaMKIIα W403L hub and CaMKIIα 6x hub (containing the six mutations Thr354Asn, Glu355Gln, Thr412Asn, Ile414Met, Ile464His, and Phe467Met) were expressed and purified as previously described (Hoelz et al. 2003; McSpadden et al. 2019; Leurs et al. 2021). In brief, recombinant CaMKIIα hub domains with an *N*-terminal 6x His-precision protease expression tag were inserted into pSKB2 (6x hub) and pET28a (WT

hub and W403L hub) vectors with kanamycin resistance, respectively. The proteins were expressed in BL21 (DE3) *E. coli* cells and purified by His-tag protein capture to nickel IMAC columns (HisTrap FF) and eluted using 75% 25 mM Tris, 150 mM KCl, 1M imidazole, 10% glycerol, pH 8.5. The proteins were buffer exchanged into a buffer containing 25 mM Tris, 150 mM KCl, 10 mM imidazole, 1 mM DTT, 10% glycerol, pH 8.5 using a HiPrep 26/10 column before precision protease was added overnight to remove the 6x His-tag. Lastly, the proteins were further purified using reverse HisTrap and size exclusion chromatography (Superose-6 gel filtration column). All purification steps were performed at 4 °C and all columns were purchased from Cytiva.

**4. Surface plasmon resonance.**

SPR measurements were performed at 25 °C using a Pioneer FE instrument (Sartorius). Recombinant CaMKIIα WT hub, CaMKIIα 6x hub, CaMKIIα W403L hub, and CaMKIIα holoenzyme (#02-109, Carna Biosciences) were immobilized by amine coupling on to a biosensor using 20 mM NaAc, pH 5 buffer. PIPA was injected in 2-fold dilution series over the immobilized CaMKIIα hub constructs using a MES running buffer (20 mM MES, 150 mM NaCl, 1 mM DTT, pH 6) and CaMKIIα holoenzyme using an HBS-P running buffer (10 mM Hepes, 150 mM NaCl, 0.005% tween, 1 mM DTT, pH 7.4). The data was analyzed using Qdat Data Analysis Tool version 2.6.3.0 (Sartorius). Sensorgrams were corrected for buffer bulk effects and unspecific binding of the samples to the chip matrix by blank and reference surface subtraction (activated flow cell channel by injection of EDC/NHS and inactivated by injection of ethanolamine). The dissociation constants ($K_D$) were estimated by plotting responses at equilibrium ($R_{eq}$) against the injected concentration and curve-fitted to a Langmuir (1:1) binding isotherm. The calculated $K_D$ value is mean ± SEM of three individual experiments.

**5. Thermal shift assay.**

$T_m$ of CaMKIIα WT hub and CaMKIIα W403L hub were determined with and without 0.3 - 160 µM PIPA by differential scanning fluorometry (DSF), as previously described (Leurs et al. 2021). Each sample was prepared with a final concentration of 0.1 mg/mL CaMKIIα and 8x SYPRO® Orange Protein Gel Stain (Life Technologies, #S6650) in MES buffer (20 mM MES, 150 mM NaCl, 1 mM DTT, pH 6) to a volume of 25 µL/well in a 96-well qPCR plate. Fluorescence was measured on a Mx3005P qPCR system (Agilent Technologies) using 492 nm as excitation and 610 nm as emission in 85 cycles with a 1 °C temperature increase; 25-100 °C. Data analysis was performed in GraphPad Prism (v. 10). where the sigmoidal curves of normalized fluorescence intensity was fitted to the Boltzmann equation and $T_m$ values were acquired. Further, the maximum difference in $T_m$ ($\Delta T_m$ max) was found via non-linear regression (One site-Fit log$IC_{50}$) from $\Delta T_m$ of each compound concentration compared to CaMKIIα WT

hub plotted against compound concentration. Data (mean $\Delta T_m$ max values ± SEM) was obtained from three independent experiments performed in technical triplicates.

**6. ADP-Glo kinase assay.**

CaMKIIα activity was assessed using the ADP-Glo Kinase Assay kit (#V9101, Promega) with CaMKIIα holoenzyme (#PR4586C, Thermo Fisher). The kinase detection reagent and the kinase reaction buffer (40 mM Tris, 0.5 mM $CaCl_2$, 20 mM $MgCl_2$, 0.1 mg/mL BSA, 50 µM DTT, pH 7.5) was prepared according to the manufacturer. All experiments were performed with 20 µL in 384-well white polypropylene plates (#784075, Greiner). The kinase reaction was performed with a final concentration of 3 ng CaMKIIα, 25 µM ATP, 50 µM syntide-II, and varying compound and CaM concentrations. CaM curves with 1 – 1781 nM CaM were obtained in the absence or presence of 100 µM or 500 µM compound. Compound Inhibition curves were generated with 1 – 5000 µM compound and submaximal CaM (30 nM) in line with recently published effect of another CaMKIIα ligand, Ph-HTBA (Griem-Krey et al. 2022). Likewise, the chosen ATP concentration was based on previous studies (Leurs et al. 2021; Griem-Krey et al. 2022) and reduce the risk of limiting potency of ATP-competing ligands. The kinase reactions were carried out for 55 min at 37 °C. Hereafter, excess ATP was depleted by incubation with 5 µL ADP-Glo Reagent for 40 min at room temperature. Finally, 10 µL Kinase Detection Reagent was added to each well to convert ADP to ATP and measured after 30 min incubation at room temperature. Luminescence was measured on a LUMIStar Omega plate reader, and data analysis and curve fitting were performed using GraphPad (v. 9). $IC_{50}$ and $EC_{50}$ values were determined using 'log(inhibitor) vs. response with variable slope'. Individual experiments were performed in technical triplicates and all curves are pooled data (mean ± SEM) of three independent experiments.

**7. Co-crystallization of PIPA with CaMKIIα 6x hub.**

Crystals were grown via sitting drop vapor diffusion at 20 °C with reservoir solution containing 11% w/v PEG3350, 300 mM potassium acetate, pH 8.0 as previously established for CaMKIIα hub crystals (Bhattacharyya et al. 2016; McSpadden et al. 2019). PIPA was co-crystallized by preincubating the protein (16 mg/mL) with 2.65 mM PIPA for 1 hr at 20 °C. 1.5 µL sitting drops were dispensed by adding 500 nL of protein stock to 1000 nL of reservoir solution. Drops were equilibrated against 50 µL of reservoir solution. Crystals appeared in 2 weeks and were cryoprotected (11% PEG, 300mM potassium acetate pH 8.0, 25% glycerol and 2.65mM PIPA) prior to flash cooling in liquid nitrogen for data collection. For statistics on X-ray diffraction data see Table S1.

**8. X-ray structure determination.**

X-ray diffraction data was collected at the Advanced Light Source (ALS) beamline 8.2.2 at wavelength 1.0000 Å and temperature of 100 K. Data were processed with XDS (Kabsch 2010), scaled and merged with Aimless (Evans and Murshudov 2013) in the CCP4 suite (Agirre et al. 2023). The space group was $C222_1$ with cell dimensions a = 103.05 Å, b = 182.92 Å, c = 107.76 Å, $\alpha = \beta = \gamma = 90°$. Initial phases were obtained by molecular replacement using Phenix Phaser-MR (McCoy et al. 2007) and the structure of CaMKIIα 6x hub with 5-HDC (PDB entry 7REC (Leurs et al. 2021)) as search model. AutoBuild was used for model building, refinement, and density modification. Further refinement of the structure was performed using Phenix (version 13) (Liebschner et al. 2019) and Coot (Emsley et al. 2010) was used for manual model building. The CIF dictionary file for PIPA was generated using Phenix eLBOW (Moriarty et al. 2009). The $2F_o$-$F_c$ electron density for PIPA, acetate, and PEG is shown in Fig. 2. Statistics for structure refinement are available in Table S1. PyMOL (The PyMOL Molecular Graphics System, Version 2.5.2 Schrödinger, LLC) was used to prepare all structure figures. 2D ligplots were generated using the LigPlot+ software (Laskowski and Swindells 2011).

**9. Small-angle X-ray scattering.**

For the SAXS studies CaMKIIα hub proteins were buffer exchanged into a MES buffer (20 mM MES, 150 mM NaCl, 1 mM DTT, pH 6.0) without or with ligands (PIPA 200 µM, HOCPCA 1000 µM, 5-HDC 100 µM) using Zeba™ Spin Desalting Columns (Thermo Fisher Scientific, 0.5 ml 7K MWCO). The buffer capacity in the presence of ligand was checked (measured by pH meter). Dilution series were made of CaMKIIα WT hub, CaMKIIα 6x hub, and CaMKIIα W403L hub in concentrations ranging from 1 to 7 mg/mL. Several preparations were made of CaMKIIα WT hub with PIPA at different protein concentrations prior to buffer exchange. During the preparation of CaMKIIα WT hub with PIPA (sample iv) significant aggregation was visible immediately upon buffer exchange; thus, the sample was centrifuged (2 min, 4 °C, 10,000 g) and SAXS data was measured only on the soluble fraction (supernatant).

SAXS data was collected at the CPHSAXS facility (University of Copenhagen, Denmark) and at the P12 beamline operated by EMBL Hamburg at the PETRA III storage ring (DESY, Hamburg, Germany) (Blanchet et al. 2015). Data from the CPHSAXS facility was collected on a BioXolver L (Xenocs) using metal jet source (Excillum) equipped with a Pilatus3 R 300K detector (Dectris). Samples were automatically loaded using the BioCUBE sample handling robot from a 96-well tray. Initial data processing was done using BioXTAS RAW (Hopkins et al. 2017). Data from P12 was collected on a Pilatus6M detector (Dectris). Samples were loaded automatically using the ARINAX BioSAXS sample

changer and sample flow during exposure. Data reduction was done using the SASflow pipeline (Franke et al. 2012).

Scattering intensities were measured at room temperature (20-22 °C) as a function of the momentum transfer $q = (4\pi\sin\theta)/\lambda$ with $2\theta$ being the scattering angle and $\lambda$ the X-ray wavelength. Details of the individual measurements are listed in Table S3.

Images were radially averaged and overlap of the individual frames checked before averaging. Corresponding buffer measurements were subtracted and, when relevant, the data from different configurations were merged and scaled by concentration to the final data files. Primary data analysis, Guinier analyses, indirect Fourier transformation, and MW estimation were done using PRIMUS (Manalastas-Cantos et al. 2021). CRYSOL (Franke et al. 2017) was used for the evaluation of single structures against the experimental data, and for mixtures OLIGOMER (Konarev et al. 2003) was used to determine best fit and corresponding volume fractions.

The dodecamer (PDB entry 5IG3) (Bhattacharyya et al. 2016) and tetradecamer (PDB entry 6OF8) (McSpadden et al. 2019) high-resolution models were used for comparison and analysis. In addition, models of stacked dodecamers and tetradecamer were made by simple translation of the individual structures using PyMOL (The PyMOL Molecular Graphics System, Version 2.5.2 Schrödinger, LLC).

**10. Mass photometry.**

Mass photometry experiments were performed on a Refeyn One MP. Standard calibration was performed using 2.25 nM apoferritin, 15 nM bovine serum albumin, and 15 nM thioglycolic acid with known molecular weights: 440 Da, 66.5 Da, and 92.11 Da, respectively. 3 µL of standard protein was diluted with 17 µL of filtered buffer (25 mM Tris-HCL, 150 mM KCl, pH 8.0) and measured for 60 sec. For experiments without PIPA, CaMKIIα WT hub and CaMKIIα W403L hub were diluted to final concentrations of 500 nM, 200 nM, and 100 nM in MES buffer (20 mM MES, 150 mM NaCl, 1 mM DTT, pH 6.0) and measurements were made for 60 sec. For experiments with PIPA added, 1.5 mg/mL CaMKIIα WT hub and CaMKIIα W403L hub were incubated with 200 µM PIPA for 90 min and desalted into MES buffer + PIPA (ZebaTM spin, 7K MWCO). The eluant was diluted to 500 nM, 200 nM, and 100 nM for each measurement. Buffer alone was measured before each measurement and histograms were generated using the Refeyn's DiscoverMP software.

**11. Intrinsic tryptophan fluorescence assay.**

ITF measurements targeting the Trp403 was were recorded at 25 °C on a Safire2 plate reader (Tecan) and performed as previously described (Leurs et al. 2021). Trp403, was previously validated as the

only Trp in the CaMKIIα hub affected upon GHB ligand binding (Trp455 and Trp462 are unaffected) (Leurs et al. 2021). Thus, the fluorescence quenching upon ligand binding observed in this assay, is directly proportional to movement of only this residue. All measurements were performed in black half-area 96-well format low-binding OptiPlates (#6052260, PerkinElmer) for fluorescence and half-area UV-Star microplates (#675801, Greiner Bio-One) for absorbance. All measurements were recorded at 25 °C on a Safire2 plate reader (Tecan). Emission was recorded in the wavelength range of 300-450 nm with 1 nm increments and an excitation wavelength of 290 nm with 5 nm bandwidths. Fluorescence intensities at 340 nm were used for data analysis. To check for inner filter correction, the absorbance was measured in the range of 270-400 nm. PIPA showed absorbance for the higher concentrations and was corrected for inner filter effect with a factor between 0.99-1.4 calculated from: $(F_{obs} - B) * 10^{0.5*h(A_{ex}+A_{em})}$.

The fluorescence intensities were normalized according to: $\frac{(F_{obs}-F_b)-F_{min}}{F_{max}-F_{min}}$

$F_{obs}$ is the observed fluorescence intensity and $F_b$ is the background fluorescence for compound in buffer alone. $F_{max}$ is the fluorescence intensity of CaMKIIα hub alone without compound, and $F_{min}$ is the fluorescence intensity when plateau is reached at high compound concentrations in the presence of the CaMKIIα hub domain. Since PIPA did not reach a plateau at high compound concentrations, $F_{min}$ was set to the fluorescence intensity of buffer for all compounds tested. Fluorescence intensities usually spanned from 3,000-40,000 for PIPA, while the fluorescence intensity for buffer was around 1,000. Non-linear regression was used for curve-fitting using the equation for 'log(inhibitor) vs. response with variable slope' to determine $IC_{50}$ values (GraphPad Prism, v. 8).

## Tables

**Table S1.** Data collection and refinement statistics for the crystal structure of CaMKIIα 6x hub with PIPA.

| | |
|---|---|
| **Crystal data** | |
| Space group | *C 2 2 $2_1$* |
| Unit cell axes *a, b, c* (Å) | 103.05, 182.92, 107.76 |
| Unit cell axes *α, β*, γ (°) | 90, 90, 90 |
| Molecules in a.u.[a] | 7 |
| **Data collection** | |
| Beamline | ALS beamline 8.2.2 |
| Wavelength (Å) | 1.0000 |
| Resolution (Å) | 46.48-2.10 (2.16-2.10)[b] |
| No. of unique reflections | 59,633 (4,582)[b] |
| Average multiplicity | 14.8 (15.0)[b] |
| Completeness (%) | 100 (100)[b] |
| $R_{pim}$ (%) | 2.9 (63.7)[b] |
| Mean I/σ(I) | 14.4 (1.3)[b] |
| Wilson B (Å$^2$) | 48.3 |
| $CC_{1/2}$ | 1 (0.58)[b] |
| **Refinement** | |
| Amino-acid residues built (subunit A/B/C/D/E/F/G) | 132/133/132/132/133/132/130 |
| PIPA/acetate/PEG/water | 2/6/1/102 |
| $R_{work}/R_{free}$ (%) | 22.4/25.1[c] |
| *Average B values (Å$^2$) for:* | |
| Amino-acid residues (subunit A/B/C/D/E/F/G) | 85.1/86.9/94.8/99.8/77.2/70.4/72.9 |
| PIPA/acetate/PEG/water | 77.2/60.0/91.9/57.7 |
| RMSD bond length (Å)/angles (°) | 0.003/0.64 |
| Ramachandran outliers/favored (%) | 0.0/97.6[d] |
| Rotamer outliers (%) /Cβ outliers (%) /Clash score | 0.3/0/6.6[d] |

[a] a.u: asymmetric unit of the crystal
[b] Outershell values are shown in parentheses
[c] $R_{free}$ is equivalent to $R_{work}$, but calculated with 5 % of reflections omitted from the refinement process
[d] MolProbity statistics from Phenix

**Table S2.** Volume fractions from the OLIGOMER fits shown in Fig. S5B.
Volume fractions larger than 2 SD are highlighted in bold. The models are listed by number of dodecamers, e.g., d4 consists of four stacked dodecamers.

| | WT hub + PIPA (i) | WT hub + PIPA (ii) | WT hub + PIPA (iii) | WT hub + PIPA (iv) | WT hub + PIPA (ii) remeasure |
|---|---|---|---|---|---|
| $\chi^2$ | 1.29 | 5.62 | 5.94 | 2.45 | 4.43 |
| **dodecamer** | **0.820±0.007** | **0.682±0.003** | **0.623±0.003** | **0.367±0.002** | **0.717±0.002** |
| **d2** | **0.097±0.014** | **0.184±0.006** | **0.095±0.005** | **0.149±0.007** | 0 |
| **d3** | 0 | 0 | 0.031±0.007 | 0.102±0.007 | 0 |
| **d4** | 0 | 0 | 0 | 0. | 0 |
| **d5** | 0 | 0 | 0 | 0 | 0 |
| **d6** | 0 | 0 | 0 | 0 | 0 |
| **d7** | 0 | 0 | 0 | **0.053±0.020** | 0 |
| **d8** | 0 | 0 | 0 | 0 | 0 |
| **d9** | 0 | 0 | 0 | 0.017±0.032 | 0 |
| **d10** | 0 | 0 | 0 | 0 | 0 |
| **d11** | 0 | 0 | 0 | **0.234±0.031** | 0 |
| **d12** | 0 | 0 | 0 | 0 | 0 |
| **d13** | 0 | 0.043±0.023 | **0.229±0.018** | 0.033±0.019 | 0 |
| **d14** | 0 | 0 | 0 | 0 | 0 |
| **d15** | 0 | **0.078±0.023** | 0.023±0.017 | 0 | 0 |
| **d16** | **0.064±0.023** | 0 | 0 | 0 | 0 |
| **d20** | 0.040±0.023 | 0.012±0.007 | 0 | 0 | 0 |
| **d24** | 0.005±0.015 | 0 | 0 | 0 | 0 |
| **d32** | 0 | 0 | 0 | 0.001±0.005 | 0 |
| **d40** | 0 | 0 | 0 | **0.044±0.005** | **0.283±0.001** |

**Table S3.** SAXS data collection details on the CaMKIIα hub domains without and with compounds.

| Sample (all hub domains) | Conc. (mg/mL) | Facility | Wavelength (Å) | Detector distance (m) | Exposure time | Measured q range ($Å^{-1}$)* |
|---|---|---|---|---|---|---|
| WT | 6.1 | P12 | 1.2398 | 3.0 | 40 x 0.090 s | 0.00224-0.734 |
| WT | 4.6 | CPHSAXS | 1.3428 | 1.0355 (S) | 10 x 60 s (S) | 0.01173-0.306 |
| WT | 2.3 | CPHSAXS | 1.3428 | 1.0355 (S) | 10 x 60 s (S) | 0.01173-0.306 |
| WT | 1.1 | CPHSAXS | 1.3428 | 1.0355 (S) | 10 x 60 s (S) | 0.01173-0.306 |
| WT<br>+ HOCPCA | 2.9 | CPHSAXS | 1.3428 | 0.610 (M)<br>1.0355 (S)<br>1.4355 (E) | 10 x 60 s (M)<br>10 x 60 s (S)<br>10 x 120 s (E) | 0.00559-0.306 |
| WT<br>+ 5-HDC | 3.4 | P12 | 1.2398 | 3.0 | 40 x 0.09 s | 0.00224-0.734 |
| WT<br>+ PIPA (i) | 1.2 | CPHSAXS | 1.3402 | 0.6325 (M)<br>1.4558 (E) | 40 x 60 s (M)<br>60 x 120 s (E) | 0.0027-0.508 |
| WT<br>+ PIPA (ii)** | 2.4 | CPHSAXS | 1.3404 | 0.6325 (M) | 40 x 60 s (M) | 0.0159-0.513 |
| WT<br>+ PIPA (ii)**<br>Remeasure after 12 h | 2.4 | CPHSAXS | 1.3404 | 0.6325 (M) | 40 x 60 s (M) | 0.0159-0.513 |
| WT<br>+ PIPA (iii)** | 3.9 | CPHSAXS | 1.3404 | 0.6325 (M) | 40 x 60 s (M) | 0.0159-0.513 |
| WT<br>+ PIPA (iv)*** | 2.3 | P12 | 1.2400 | 3.0 | 30 x 0.095 s | 0.00205-0.447 |
| 6x | 3.4 | P12 | 1.2398 | 3.0 | 40 x 0.090 s | 0.00224-0.734 |
| 6x | 4.2 | CPHSAXS | 1.3428 | 1.0355 (S) | 10 x 60 s (S) | 0.01173-0.306 |
| 6x | 2.1 | CPHSAXS | 1.3428 | 1.0355 (S) | 10 x 60 s (S) | 0.01173-0.306 |
| 6x | 1.1 | CPHSAXS | 1.3428 | 1.0355 (S) | 10 x 60 s (S) | 0.01173-0.306 |
| 6x<br>+ 5-HDC | 4.4 | CPHSAXS | 1.3428 | 1.0355 (S)<br>1.4355 (E) | 10 x 60 s (S)<br>10 x 120 s (E) | 0.00559-0.306 |
| 6x<br>+ PIPA | 6.7 | CPHSAXS | 1.3402 | 0.6325 (M)<br>1.4558 (E) | 40 x 60 s (M)<br>60 x 120 s (E) | 0.0027-0.508 |
| W403L | 6.4 | P12 | 1.2400 | 3.0 | 30 x 0.095 s | 0.00205-0.447 |
| W403L<br>+ 5-HDC | 6.0 | CPHSAXS | 1.3402 | 0.6325 (M)<br>1.4558 (E) | 40 x 60 s (M)<br>60 x 120 s (E) | 0.0027-0.508 |
| W403L<br>+ PIPA | 6.8 | P12 | 1.2400 | 3.0 | 30 x 0.095 s | 0.00205-0.447 |

*Data collected. Subsequently cropped with $q_{min}$ according to Guinier analyses and $q_{max}$ for additional analyses set to ≤0.4 $Å^{-1}$.

**Some sample development / heterogeneity during data collection, thus only a full average from the M setting used.

***Soluble fraction only, i.e., supernatant after sample with visible aggregation was centrifuged.

## Figures

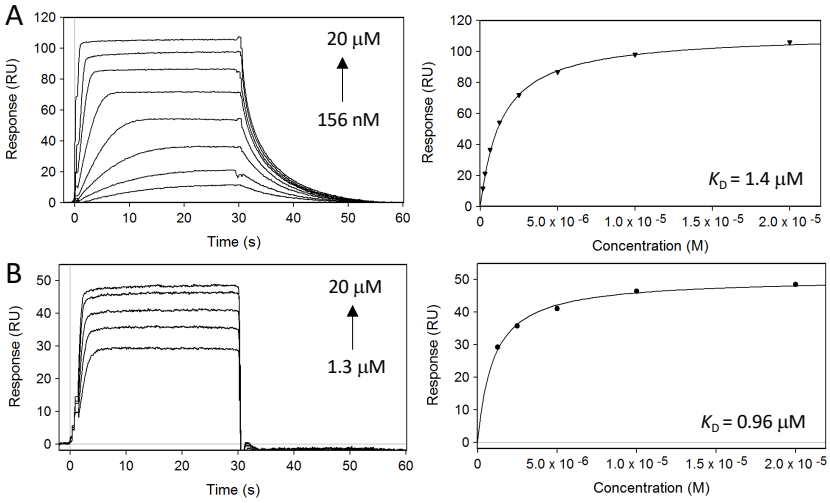


**Figure S1. Binding of PIPA to CaMKIIα 6x hub and CaMKIIα holoenzyme.**
**A)** Concentration-dependent binding of PIPA to CaMKIIα 6x hub measured by SPR (left) and SPR Langmuir-binding isotherm (right). **B)** Concentration-dependent binding of PIPA to immobilized CaMKIIα holoenzyme measured by SPR (left) and SPR Langmuir-binding isotherm (right).

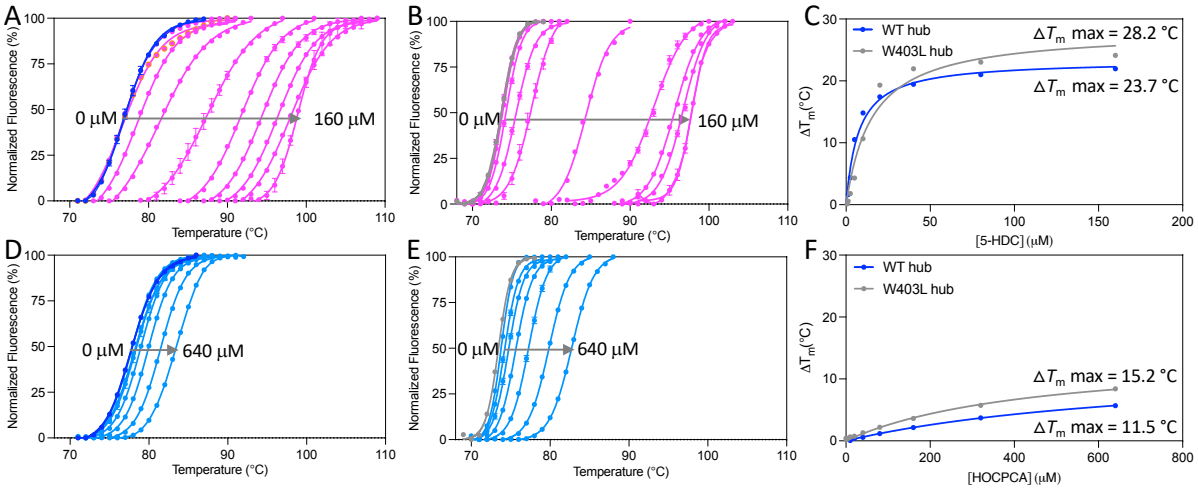


**Figure S2. Thermal shift assay on CaMKIIα hub domains.**
**A)** Right-shifted thermal shift assay melting curves of CaMKIIα WT hub upon binding of HOCPCA. **B)** Right-shifted thermal shift assay melting curves of CaMKIIα W403L hub upon binding of HOCPCA. **C)** Thermal melting point of CaMKIIα WT hub (blue) and CaMKIIα W403L hub (grey) plotted against increasing concentrations of HOCPCA (representative data of n = 3). **D)** Right-shifted thermal shift assay melting curves of CaMKIIα WT hub upon binding of 5-HDC. **E)** Right-shifted thermal shift assay melting curves of CaMKIIα W403L hub upon binding of 5-HDC. **F)** Thermal melting point of CaMKIIα WT hub (blue) and CaMKIIα W403L hub (grey) plotted against increasing concentrations of 5-HDC (representative data of n = 3).

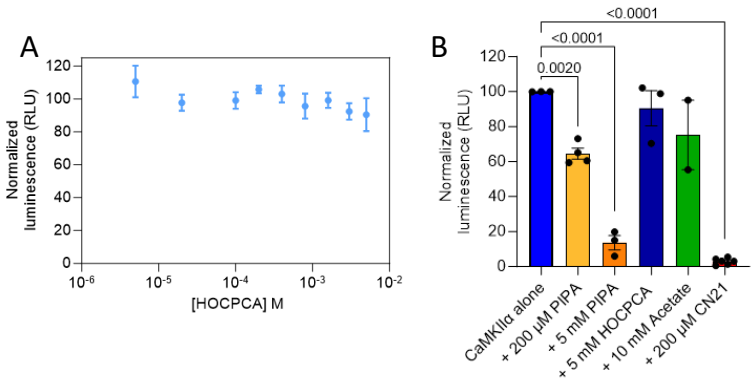


**Figure S3. Inhibition of CaMKIIα syntide-2 phosphorylation.**
**A)** No concentration-dependent inhibition of CaMKIIα syntide-2 phosphorylation by HOCPCA using sub-maximal (30 nM) CaM concentrations, investigated with the luminescence-based ADP-Glo kinase assay (n = 3, mean ± SEM). **B)** Comparison of kinase inhibition by PIPA (200 µM and 5 mM), HOCPCA (5 mM), acetate (10 mM), and CN21 (200 µM) (n = 2-4, mean ± SEM).

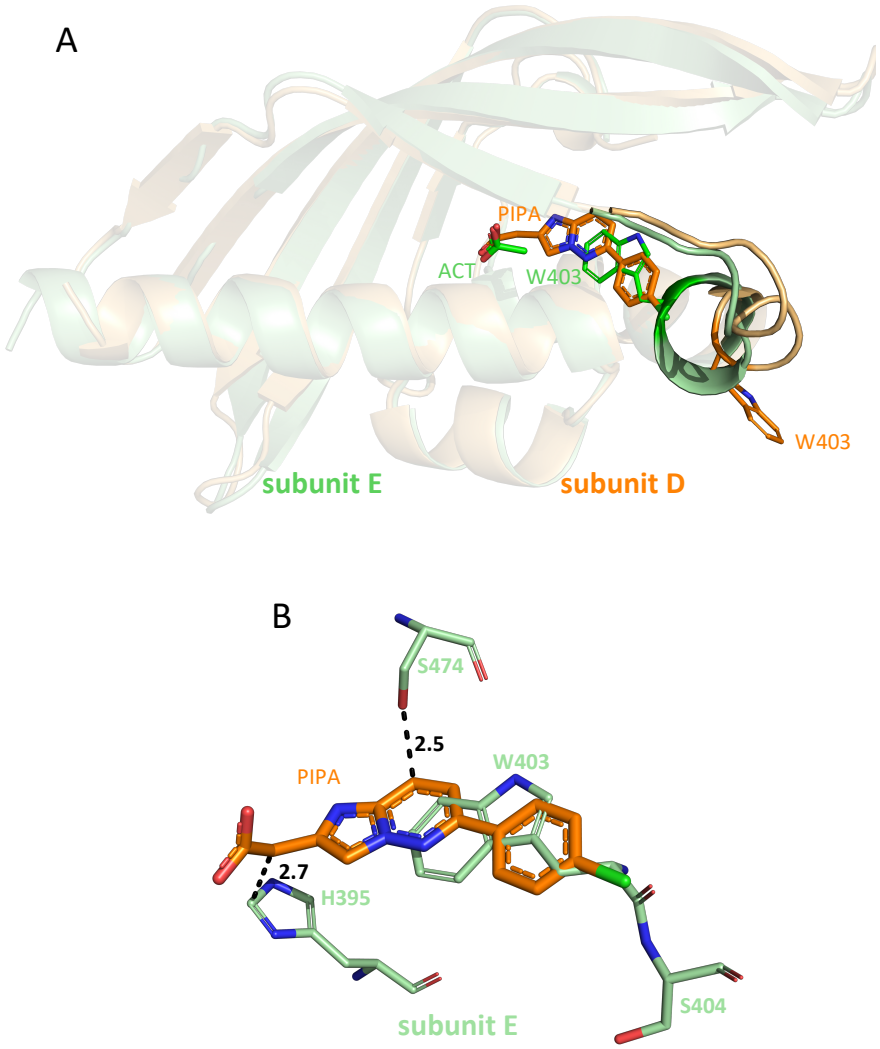


**Figure S4. Structural inferences upon PIPA binding.**
**A)** Superimposition of CaMKIIα 6x hub subunits with acetate (ACT) (subunit E; light green) and PIPA (subunit D; light orange), respectively. The subunits are shown as cartoon representation with ACT (green carbon atoms), PIPA (orange carbon atoms), and Trp403 (subunit E: dark green and subunit D: dark orange) shown as sticks. **B)** PIPA would severely clash with W403 and S404 in the inwards flipped conformation (subunit E).

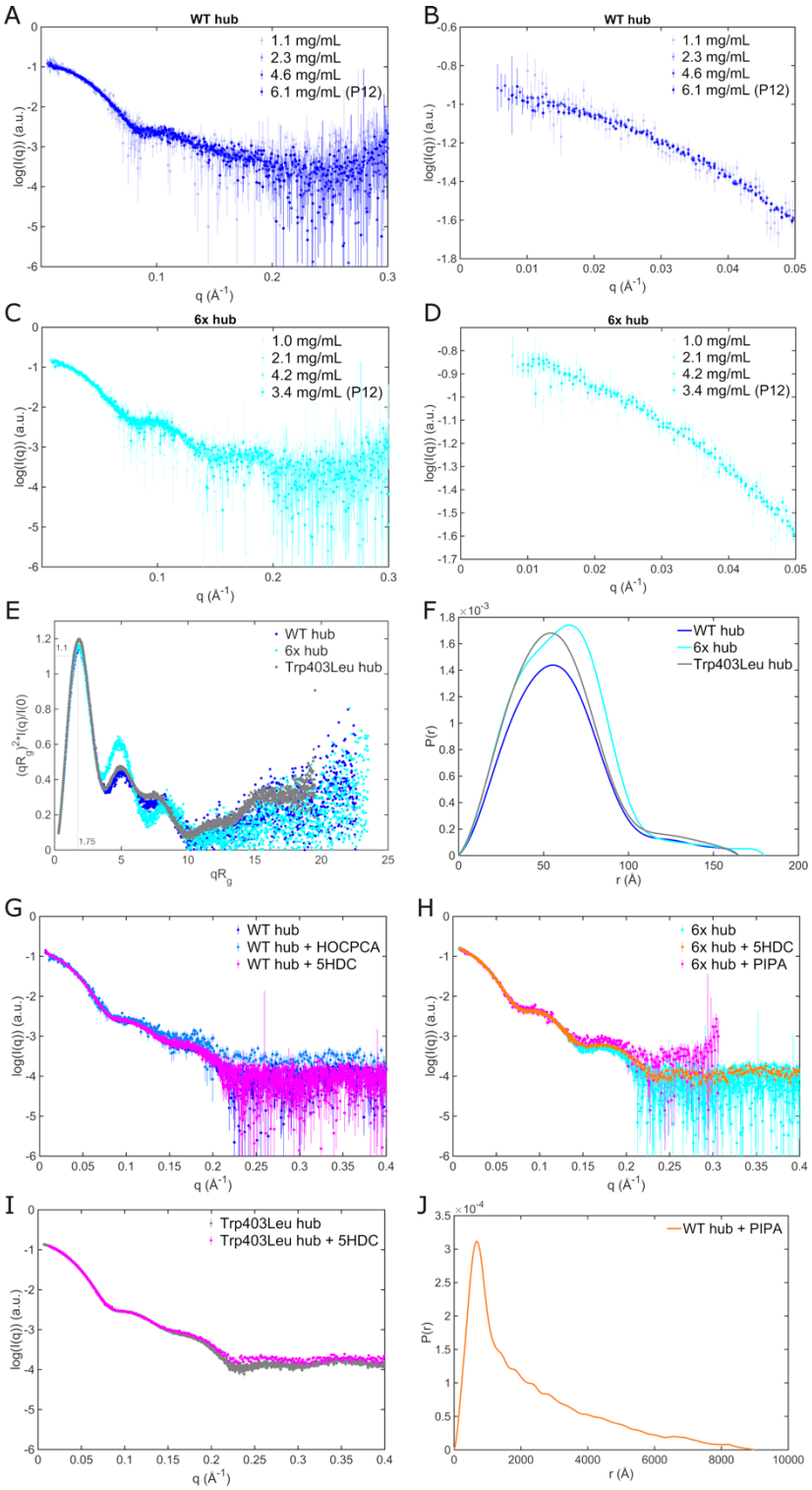


**Figure S5. SAXS on CaMKIIα hub domains.**

**A-B)** Scattering curves for CaMKIIα WT hub at different concentrations and from both lab source (unmarked) and synchrotron (P12). **C-D)** Scattering curves of CaMKIIα 6x hub at different concentrations and from both lab source (unmarked) and synchrotron (P12). **E)** Kratky plots of CaMKIIα WT, 6x, and W403L hub domains. **F)** CaMKIIα WT, 6x, and W403L hub domains pair distance distribution functions. **G)** CaMKIIα WT hub without and with compounds (1000 mM HOCPCA and 100 mM 5-HDC). **H)** Scattering curves of CaMKIIα 6x hub without and with compounds (200 mM PIPA and 100 µM 5-HDC). **I)** Scattering curves of CaMKIIα W403L hub without and with 100 mM 5HDC). **J)** Pair-distance distribution function for CaMKIIα WT hub with PIPA.

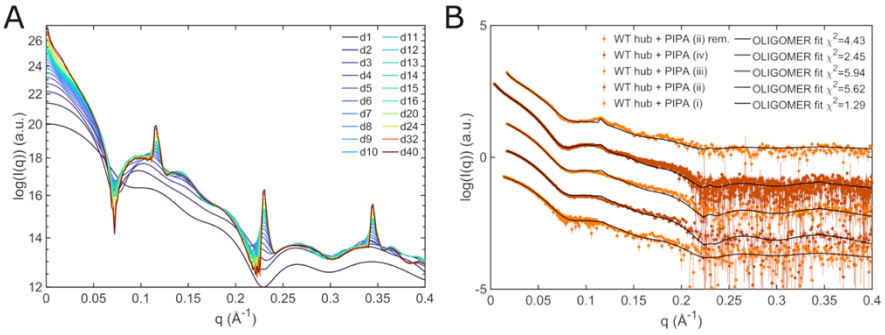


**Figure S6. Models of self-association and corresponding fits to SAXS data.**
**A**) Theoretical scattering curves for stacked dodecamers of CaMKIIα hub domain structures used in the OLIGOMER pool. The curves are ordered by number of dodecamers in the respective model, e.g., d4 consists of four stacked dodecamers. All models are based on PDB entry 5IG3, as illustrated in Fig. 3E. **B)** Fits to SAXS data of CaMKIIα WT hub with PIPAobtained from OLIGOMER with different distributions of self-associated stacks (cf Table S2). The scattering curves have been translated for clarity.

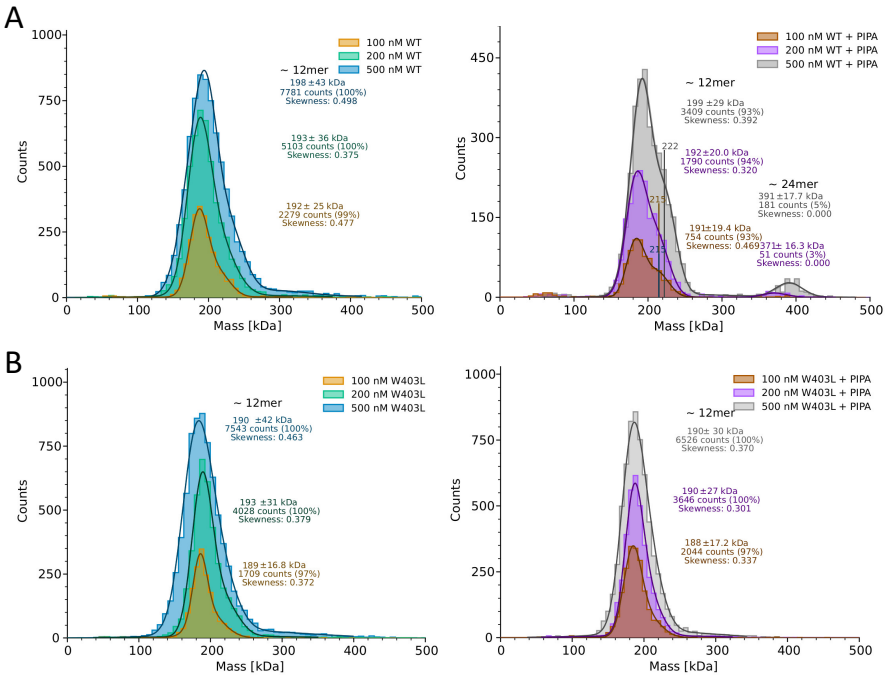


**Figure S7. MP histograms of CaMKIIα WT hub and CaMKIIα W403L hub.**
**A)** Representative MP histograms showing CaMKIIα WT hub diluted to 500 nM, 200 nM and 100 nM without (left) and with the addition of PIPA (right). **B)** Representative MP histograms of CaMKIIα W403L hub diluted to 500 nM, 200 nM, and 100 nM without (left) and with the addition of PIPA (right). Each count indicates a single molecule.

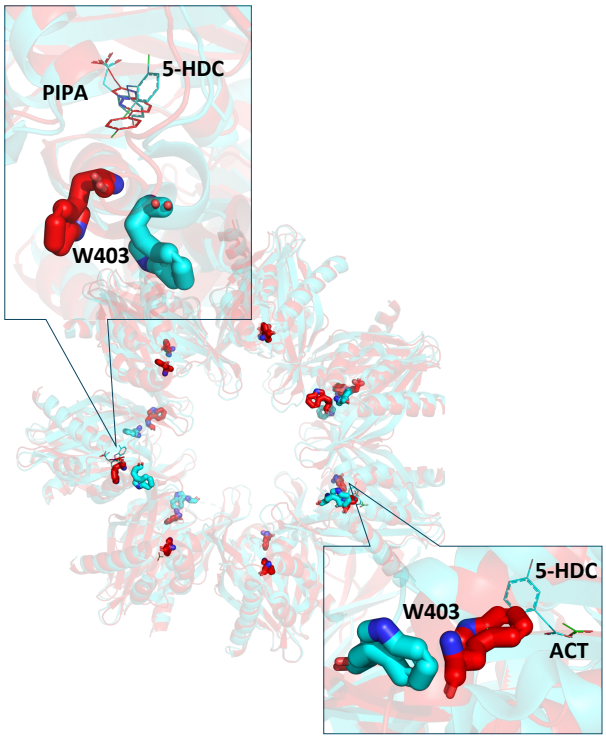


**Figure S8. Comparison of CaMKIIα 6x hub structures with PIPA and 5-HDC.**
Superimposed X-ray structures (PDB entry 7REC) of tetradecameric CaMKIIα 6x hub (14-mer generated from 7-mer) with PIPA (red) and 5-HDC (cyan). The proteins are shown as cartoon. Zoomed-in (top left) view shows the binding site of CaMKIIα 6x hub compounds (PIPA and 5-HDC) as lines and the corresponding Trp403 positioned outwards in sticks representation. Zoomed-in (bottom right) view shows the binding site of CaMKIIα 6x hub compounds (acetate (red) and 5-HDC) as lines and the corresponding Trp403 flipped inward (acetate)/outward (5-HDC).

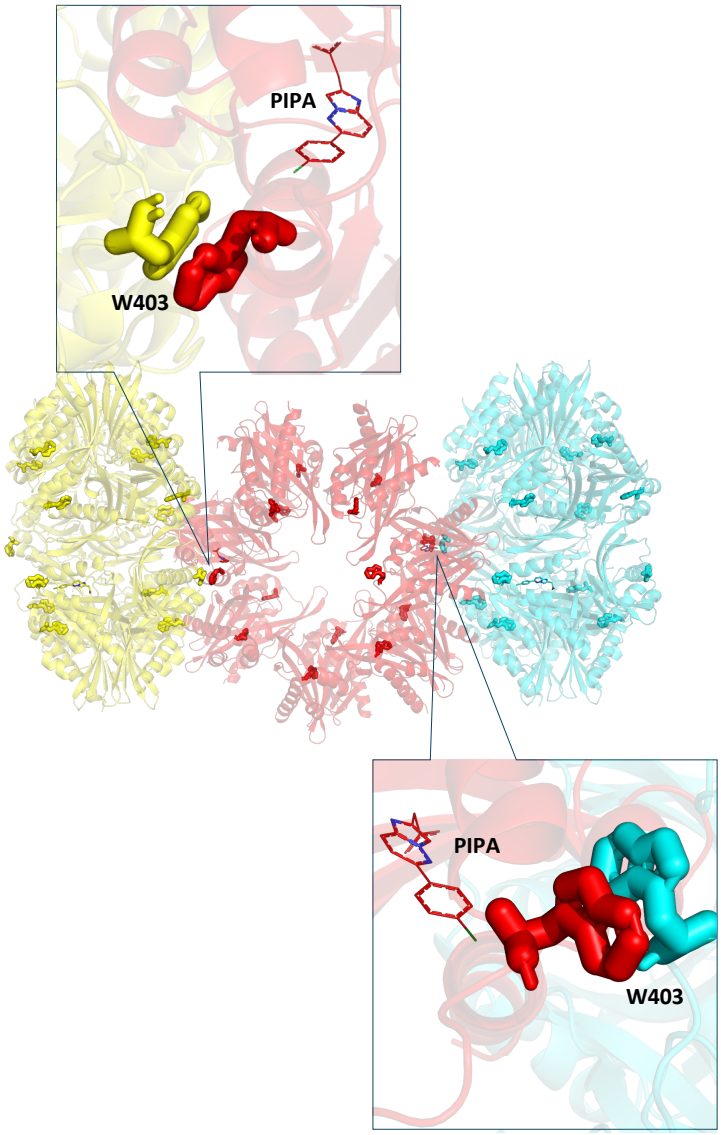


**Figure S9. Face-to-edge crystal packing of tetradecameric CaMKIIα 6x hub with PIPA.**
Crystal packing of tetradecameric CaMKIIα 6x hub with PIPA shown as cartoon. Zoomed-in (top left and bottom right) views show the binding site for CaMKIIα 6x hub compounds (here PIPA) in red line representation and Trp403 in sticks representation. Trp403 from the corresponding symmetry mates are colored yellow and cyan.

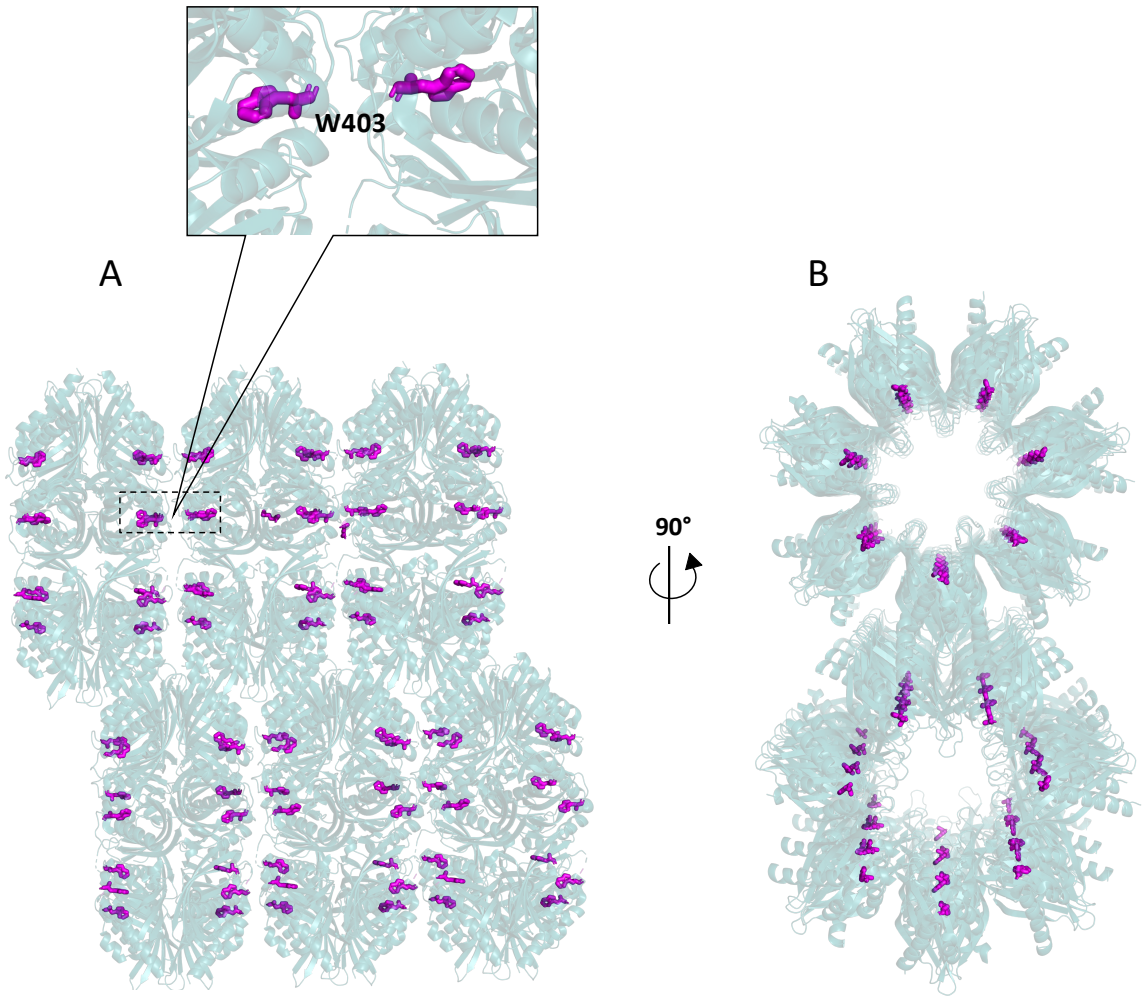


**Figure S10. Stacked crystal packing of tetradecameric CaMKIIα 6x hub.**
Crystal packing of tetradecameric CaMKIIα 6x hub (PDB entry 6OF8) shown as transparent dark cyan cartoon and Trp403 in magenta stick representation. **A)** CaMKIIα 6x hub oligomer packing in the crystal structure, with zoom-in view on two Trp403 in the adjacent subunits of CaMKIIα 6x hub tetradecamer. **B)** Corresponding top view of the CaMKIIα 6x hub crystal packing.

## SI References


Agirre J, Atanasova M, Bagdonas H, Ballard CB, Basle A, Beilsten-Edmands J, Borges RJ, Brown DG, Burgos-Marmol JJ, Berrisford JM, Bond PS, Caballero I, Catapano L, Chojnowski G, Cook AG, Cowtan KD, Croll TI, Debreczeni JE, Devenish NE, Dodson EJ, Drevon TR, Emsley P, Evans G, Evans PR, Fando M, Foadi J, Fuentes-Montero L, Garman EF, Gerstel M, Gildea RJ, Hatti K, Hekkelman ML, Heuser P, Hoh SW, Hough MA, Jenkins HT, Jimenez E, Joosten RP, Keegan RM, Keep N, Krissinel EB, Kolenko P, Kovalevskiy O, Lamzin VS, Lawson DM, Lebedev AA, Leslie AGW, Lohkamp B, Long F, Maly M, McCoy AJ, McNicholas SJ, Medina A, Millan C, Murray JW, Murshudov GN, Nicholls RA, Noble MEM, Oeffner R, Pannu NS, Parkhurst JM, Pearce N, Pereira J, Perrakis A, Powell HR, Read RJ, Rigden DJ, Rochira W, Sammito M, Sanchez Rodriguez F, Sheldrick GM, Shelley KL, Simkovic F, Simpkin AJ, Skubak P, Sobolev E, Steiner RA, Stevenson K, Tews I, Thomas JMH, Thorn A, Valls JT, Uski V, Uson I, Vagin A, Velankar S, Vollmar M, Walden H, Waterman D, Wilson KS, Winn MD, Winter G, Wojdyr M, Yamashita K. The CCP4 suite: integrative software for macromolecular crystallography. Acta Crystallographica Section D. 2023;79:449-461.

Bhattacharyya M, Stratton MM, Going CC, McSpadden ED, Huang Y, Susa AC, Elleman A, Cao YM, Pappireddi N, Burkhardt P, Gee CL, Barros T, Schulman H, Williams ER, Kuriyan J. Molecular mechanism of activation-triggered subunit exchange in Ca(2+)/calmodulin-dependent protein kinase II. Elife. 2016;5.

Blanchet CE, Spilotros A, Schwemmer F, Graewert MA, Kikhney A, Jeffries CM, Franke D, Mark D, Zengerle R, Cipriani F, Fiedler S, Roessle M, Svergun DI. Versatile sample environments and automation for biological solution X-ray scattering experiments at the P12 beamline (PETRA III, DESY). J Appl Crystallogr. 2015;48:431-443.

Emsley P, Lohkamp B, Scott WG, Cowtan K. Features and development of Coot. Acta Crystallogr D Biol Crystallogr. 2010;66:486-501.

Evans PR, Murshudov GN. How good are my data and what is the resolution? Acta Crystallogr D Biol Crystallogr. 2013;69:1204-1214.

Franke D, Kikhney AG, Svergun DI. Automated acquisition and analysis of small angle X-ray scattering data. Nuclear Instruments and Methods in Physics Research Section A: Accelerators, Spectrometers, Detectors and Associated Equipment. 2012;689:52-59.

Franke D, Petoukhov MV, Konarev PV, Panjkovich A, Tuukkanen A, Mertens HDT, Kikhney AG, Hajizadeh NR, Franklin JM, Jeffries CM, Svergun DI. ATSAS 2.8: a comprehensive data analysis suite for small-angle scattering from macromolecular solutions. J Appl Crystallogr. 2017;50:1212-1225.

Griem-Krey N, Gauger SJ, Gowing EK, Thiesen L, Frølund B, Clarkson AN, Wellendorph P. The CaMKIIα hub ligand Ph-HTBA promotes neuroprotection after focal ischemic stroke by a distinct molecular interaction. Biomed Pharmacother. 2022;156:113895.

Hoelz A, Nairn AC, Kuriyan J. Crystal structure of a tetradecameric assembly of the association domain of Ca2+/calmodulin-dependent kinase II. Mol Cell. 2003;11:1241-1251.

Hopkins JB, Gillilan RE, Skou S. BioXTAS RAW: improvements to a free open-source program for small-angle X-ray scattering data reduction and analysis. J Appl Crystallogr. 2017;50:1545-1553.

Kabsch W. Xds. Acta Crystallogr D Biol Crystallogr. 2010;66:125-132.

Konarev PV, Volkov VV, Sokolova AV, Koch MHJ, Svergun DI. PRIMUS: a Windows PC-based system for small-angle scattering data analysis. J Appl Crystallogr. 2003;36:1277-1282.

Laskowski RA, Swindells MB. LigPlot+: Multiple Ligand–Protein Interaction Diagrams for Drug Discovery. Journal of Chemical Information and Modeling. 2011;51:2778-2786.

Leurs U, Klein AB, McSpadden ED, Griem-Krey N, Solbak SMØ, Houlton J, Villumsen IS, Vogensen SB, Hamborg L, Gauger SJ, Palmelund LB, Larsen ASG, Shehata MA, Kelstrup CD, Olsen JV, Bach A, Burnie RO, Kerr DS, Gowing EK, Teurlings SMW, Chi CC, Gee CL, Frølund B, Kornum BR, van Woerden GM, Clausen RP, Kuriyan J, Clarkson AN, Wellendorph P. GHB analogs confer

neuroprotection through specific interaction with the CaMKIIα hub domain. Proc Natl Acad Sci U S A. 2021;118.

Liebschner D, Afonine PV, Baker ML, Bunkoczi G, Chen VB, Croll TI, Hintze B, Hung LW, Jain S, McCoy AJ, Moriarty NW, Oeffner RD, Poon BK, Prisant MG, Read RJ, Richardson JS, Richardson DC, Sammito MD, Sobolev OV, Stockwell DH, Terwilliger TC, Urzhumtsev AG, Videau LL, Williams CJ, Adams PD. Macromolecular structure determination using X-rays, neutrons and electrons: recent developments in Phenix. Acta Crystallogr D Struct Biol. 2019;75:861-877.

Manalastas-Cantos K, Konarev PV, Hajizadeh NR, Kikhney AG, Petoukhov MV, Molodenskiy DS, Panjkovich A, Mertens HDT, Gruzinov A, Borges C, Jeffries CM, Svergun DI, Franke D. ATSAS 3.0: expanded functionality and new tools for small-angle scattering data analysis. J Appl Crystallogr. 2021;54:343-355.

McCoy AJ, Grosse-Kunstleve RW, Adams PD, Winn MD, Storoni LC, Read RJ. Phaser crystallographic software. J Appl Crystallogr. 2007;40:658-674.

McSpadden ED, Xia Z, Chi CC, Susa AC, Shah NH, Gee CL, Williams ER, Kuriyan J. Variation in assembly stoichiometry in non-metazoan homologs of the hub domain of Ca(2+) /calmodulin-dependent protein kinase II. Protein Sci. 2019;28:1071-1082.

Moriarty NW, Grosse-Kunstleve RW, Adams PD. electronic Ligand Builder and Optimization Workbench (eLBOW): a tool for ligand coordinate and restraint generation. Acta Crystallogr D Biol Crystallogr. 2009;65:1074-1080.